The Analysis of the Ice Edge Position Variability in the Arctic Seas Depending on Different Types of Winter Severity

M. S. Teider, N. S. Frolova, N. A. Podrezova, and K. V. Kravtsova

Abstract The article presents the results of research on the ice cover changes in the Arctic basin according to the satellite data. Light cloud cover satellite images of the MODIS spectroradiometer were used to estimate the parameters of the ice cover of the Arctic seas. QueryThe images of the Landsat-8 satellite were used to refine the data obtained from the MODIS spectroradiometer (Terra satellite) because of their better spatial resolution. The classification according to the severity of winter seasons for the White, Kara, Laptev and East Siberian Seas is also described in the article.

Keywords Arctic · Sea ice area · Sea ice concentration · Fast ice width · Sea ice edge · Severity of winter seasons

The introduction of remote sensing from Space has presented new opportunities in the study of the ice cover of the Arctic seas. The use of satellites has undeniable advantages due to their significant spatial coverage tied to a coordinate grid and short time interval of measurements.

It is also worth considering that in the harsh conditions of the Arctic, contact measurements are quite difficult to carry out, and in some areas it is simply impossible. Currently, remote sensing data is an indispensable source of information for conducting production and research activities in the Arctic region. With the help of remote sensing, through the analysis of the ice situation, the issues of navigation support and economic activity and the tasks of determining the total area, concentration and climatology of ice formations are solved. Remote sensing methods are divided into the following types: passive methods which record thermal, visible and natural gamma radiation from the water surface; semi-active methods which analyze the signal received after irradiation of the sea by an electromagnetic radiation source in a wide spectral range; active methods which register reflected radiation, fluorescence, or combination scattering after irradiation by a radiation source at a given spectral composition [1].

M. S. Teider · N. S. Frolova · N. A. Podrezova (✉) · K. V. Kravtsova
Russian State Hydrometeorological University, St. Petersburg, Russia
e-mail: Nadinapod@mail.ru

V. I. Karev (ed.), *Physical and Mathematical Modeling of Earth and Environment Processes—2022*, Springer Proceedings in Earth and Environmental Sciences,
https://doi.org/10.1007/978-3-031-25962-3_11

The visible range is the part of the electromagnetic spectrum that is perceived by the human eye (0.4–0.7 μm). Sensing in this range is carried out using various satellites with different temporal and spatial resolution. Obtained in cloudless and well-lit conditions, the images allow us to identify various characteristics of the ice cover, such as cracks, chips, shape, etc., and thereby contribute to the attribution of ice floes to a certain type. However, there is no possibility of sensing in the conditions of the polar night, and the daytime weather conditions are often not favorable because of thick clouds. This leads to a decrease in possibility of obtaining high-resolution images, and at the same time it becomes difficult to determine the quality and development of ice floes.

The infrared range is the electromagnetic range from 0.78 to 1000 μm. Sea ice chart composition is carried out in the IR range of 10.5–12.5 μm, because spectral differences in absorption, reflection and scattering of radiant energy from ice, snow and water surfaces are maximally pronounced in this range. So, all young types of ice are well recognized.

IR sensors (in the wavelength range over 3 μm) has no restrictions on the time of day. However, thick clouds can become a strong barrier to infrared remote sensing. Temperatures above − 6 °C also have a direct effect on the sensors.

According to the obtained images, it is possible to determine the thickness and some types of ice. When the air temperature drops below zero, it means the following: the thicker the ice, the lower the surface temperature. When the air temperature rises, the ability to determine the ice thickness decreases, because the sea ice surface begins to melt. The water, produced by surface melting, prevents ice from emitting electromagnetic radiation.

In the range 1 mm–1 m the microwave brightness temperature is measured. This parameter depends on the physical properties of water and ice, such as the presence and height of snow cover, its annual evolution, radiation, and the influence of the atmosphere. The water surface has a high reflectivity and strong polarization. The radiation of annual ice is quite strong with weak polarization. Because of their long wavelengths, compared to the visible and infrared, microwaves have special properties that are important for remote sensing. Longer wavelength microwave radiation can penetrate through cloud cover, haze, dust, and rainfall. It is possible to detect microwave energy under almost all weather and environmental conditions so that data can be collected at any time. Microwave sensing includes both active and passive methods. Passive microwave sensing is similar to thermal one. The sensor detects the naturally emitted microwave energy within its field of view. This emitted energy is related to the temperature and moisture properties of the emitting object or surface. Oceanographic applications of passive microwave sensing include mapping sea ice, evaluation of sea ice concentration, and detection of ice hummocks. Active microwave sensors provide their own source of microwave radiation to illuminate the target. These sensors are generally divided into two distinct categories: imaging and non-imaging. The most common form of imaging active microwave sensors is radar. It transmits a microwave (radio) signal towards the target and detects the backscattered portion of the signal. The radar images are used to detect ice (mostly

old), determine the thickness of the ice cover and find the presence of certain types of ice formations such as icebergs and ice fields.

Non-imaging microwave sensors include altimeters and scatterometers. Radar altimeters transmit short microwave pulses (more than 1700 pulses per second) and measure the round trip time delay to targets to determine their distance from the sensor. Altimeters measure the thickness of a part of the ice above the water, the thickness and density of snow using the assessment of climatic data [1–5].

The NASA National Snow and Ice Data Center Distributed Active Archive Center (NASA NSIDC DAAC) includes near-global passive microwave data from 1978 to present [6]. These data products are derived from the Scanning Multichannel Microwave Radiometer (SMMR) instrument on the Nimbus-7 satellite and the Special Sensor Microwave/Imager (SSM/I) and Special Sensor Microwave Imager/Sounder (SSMI/S). The data have a number of errors, including underestimation of sea ice concentration of the broken ice during melting, false effects in coastal areas and zones of polar cyclones' movement, as well as the lack of data due to various spots on the images.

Light cloud cover satellite images of the MODIS spectroradiometer were used to estimate the parameters of the ice cover of the Arctic seas. MODIS has a wide field of view which allows us to determine the position of the edge and the residual forms of ice only in summer. Observation of the Arctic in polar winter is difficult because of the long-continuing darkness while the sun is below the horizon. Satellite images in the visible wavebands are not useful during polar nights. The data are selected using EOSDIS Worldview [7]. A combination of 3–6-7 "false" colors according to the RGB model was used. This combination is used to map snow and ice. Snow and ice are very reflective in the visible part of the spectrum (Band 3), and very absorbent in Bands 6 and 7 (short-wave infrared, or SWIR). This band combination is good for distinguishing liquid water from frozen water, for example, clouds over snow, ice cloud versus water cloud. Consequently, the more snow and the thicker ice, the stronger the absorption in the SWIR bands, and the more red the colour. Thick ice and snow appear vivid red (or red–orange), while small ice crystals in high-level clouds will appear reddish-orange or peach. For further work the images from Worldview were decomposed into multiple layers (Fig. 1).

The images of the Landsat-8 satellite were used to refine the data obtained from the MODIS spectroradiometer (Terra satellite) because of their better spatial resolution [8].

Ice concentration is the ratio of an area of ice to the total area of water surface within some large geographic locality. Seasonality has a significant effect on the ice conditions of the Arctic region, therefore the changes in this parameter for every summer month are considered.

The calculations of concentration were performed in the UNESCO Bilko software, where image histograms of pixel intensity corresponding to water, ice and different types of clouds were drawn for each of the Arctic seas on a monthly basis during the summer period. An example is shown in Fig. 2. The month of September was excluded from the investigation because in most seas the water surface was already

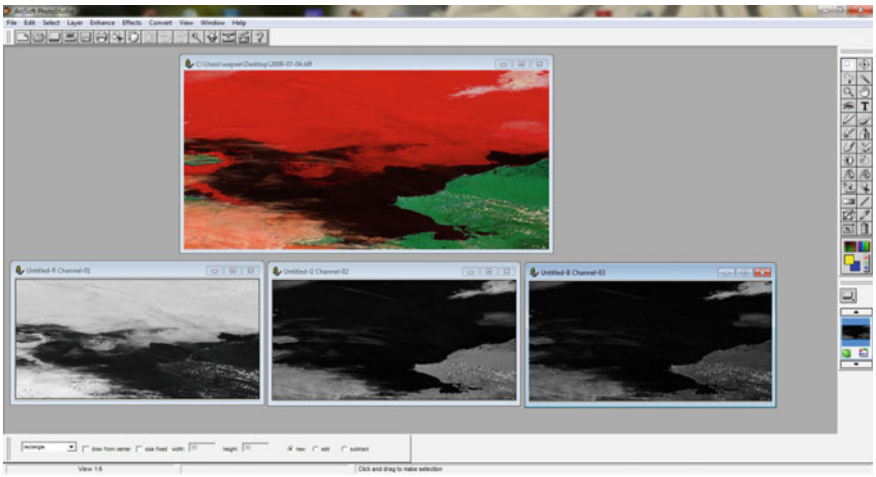

Fig. 1 Terra/MODIS satellite image of the Chukchi Sea on July 4, 2009 (top) and image decomposition in the ArcSoft PhotoStudio program (bottom)

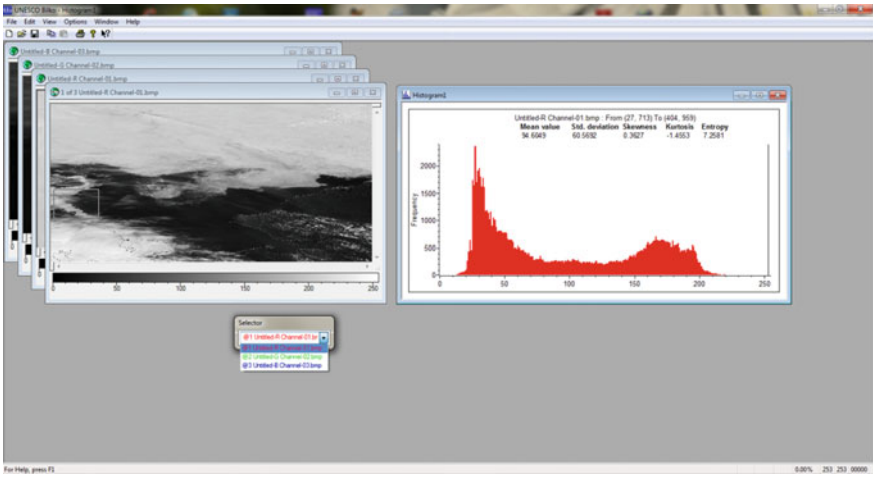

Fig. 2 Process of determining ice concentration in the Chukchi Sea (on the selected fragment) using a Bilko software histogram. Terra/MODIS composite grayscale image with combined bands (July 4, 2009)

ice-free in August. The Lincoln Sea was not included in the calculations, as the trend analysis has shown that the ice cover in this sea has not changed since 1979 [9].

The obtained results of sea ice concentration (in %) in the Arctic region for the period from 2009 to 2019 are recorded in Table 1, where 0 means absolutely clear water free of ice cover, and 100—fast ice.

Table 1 Results of ice concentration (in %) for the Arctic seas during the summer period

Year	Month	Sea											
		East Siberian	Kara	Beaufort	Laptev	Chukchi	Baffin	Barents	White	Greenland	Norwegian	Bering	Labrador
2009	*VI*	95	87	92	89	84	64	50	0	100	0	24	67
	VII	75	57	60	65	70	34	30	0	95	0	0	27
	VIII	0	0	15	30	0	5	0	0	91	0	0	0
2010	*VI*	94	84	88	76	90	62	47	0	100	0	32	57
	VII	80	60	40	59	64	55	33	0	94	0	0	14
	VIII	30	0	5	2	33	19	0	0	89	0	0	0
2011	*VI*	94	85	83	77	95	72	42	0	94	0	13	25
	VII	84	64	61	55	44	34	25	0	90	0	0	6
	VIII	0	0	13	0	0	7	0	0	85	0	0	0
2012	*VI*	88	45	76	72	88	59	34	0	96	0	77	54
	VII	72	0	20	44	67	36	0	0	78	0	0	4
	VIII	45	0	0	0	38	0	0	0	64	0	0	0
2013	*VI*	98	92	87	82	87	65	41	0	94	0	0	63
	VII	84	58	64	54	28	27	5	0	87	0	0	32
	VIII	25	0	0	0	–	0	0	0	81	0	0	11
2014	*VI*	87	91	81	68	55	–	34	0	95	0	48	58
	VII	68	60	33	38	30	48	0	0	85	0	0	20
	VIII	28	0	0	0	10	0	0	0	79	0	0	0
2015	*VI*	84	90	75	78	87	57	48	0	99	0	13	70
	VII	62	55	43	55	41	32	26	0	93	0	0	48

(continued)

Table 1 (continued)

Year	Month	Sea											
		East Siberian	Kara	Beaufort	Laptev	Chukchi	Baffin	Barents	White	Greenland	Norwegian	Bering	Labrador
	VIII	0	0	11	0	0	–	0	0	85	0	0	26
2016	*VI*	88	84	82	75	85	59	20	0	96	0	21	55
	VII	53	42	58	43	52	42	0	0	89	0	0	14
	VIII	15	0	33	0	0	12	0	0	83	0	0	0
2017	*VI*	82	75	84	72	77	52	45	0	90	0	16	67
	VII	61	45	69	44	53	38	21	0	87	0	0	39
	VIII	0	0	0	25	0	14	0	0	83	0	0	18
2018	*VI*	90	89	80	65	80	51	33	0	95	0	0	57
	VII	45	40	62	–	22	35	0	0	88	0	0	34
	VIII	0	0	55	0	0	21	0	0	81	0	0	0
2019	*VI*	80	94	52	67	83	57	47	0	97	0	5	52
	VII	20	0	33	–	35	48	14	0	82	0	0	19
	VIII	0	0	16	0	0	19	6	0	74	0	0	0

June is characterized by the maximum sea ice cover in the Arctic Ocean over the entire summer season. The high-concentration ice extends from the central and eastern part of the Siberian shelf (from the Kara Sea to the East Siberian Sea inclusive) across the entire ocean to Greenland and the Canadian Arctic Archipelago, partly including the Beaufort Sea, where the ice fields break up at this time, and the Greenland Sea shelf area. The Barents Sea ice is characterized by reduced ice concentration (20–45%). The White Sea and Norwegian Sea are completely ice-free. Relatively low concentration is observed in the Baffin and Bering Seas.

In July, total sea ice concentration continues to decrease rapidly: seas influenced by warm Atlantic waters are almost or completely cleared of ice, a significant reduction is also observed on the Siberian shelf. Ice concentration in areas belonging to the USA and Canada changes little, but the trend persists (the index decreases by 10–30%).

August is characterized by an even greater reduction in ice cover: ice has melted in the Barents and Kara Seas, and ice with a concentration of 40% remains only in the north part of the Laptev Sea—almost the entire Russian Arctic sector is free for ship navigation. The highest concentration is noted in the Greenland and Beaufort Seas [4].

Regarding the interannual variation of the parameter, a significant decrease in the Arctic sea ice concentration value is observed from 2009 to 2019. Firstly, during the summer months of this period, the White and Norwegian Seas are absolutely free of ice. The same situation is also expected in the near future in the Bering Sea, where severe ice conditions were observed only in 2012 (77%), and there was almost no ice in any other year during the period under investigation. Secondly, in the Siberian seas, the rate of melting in July has increased significantly, although the figures for June remain about the same. While the 2009 July sea ice concentration is 60–70%, in 2019 it is only 20–30%. The Greenland and Beaufort Seas are also characterized by a decrease in the monthly concentration—it has become about 1.5–2 times less. However, the situation is rather stable in the Baffin and Labrador Seas. It is possible that for these seas, the eleven-year time interval is insufficient for analysis and a longer interval is required, or the area chosen for the study is relatively stable.

A straight line cut through the combined color image was plotted in the UNESCO Bilko software in order to determine the width of the fast ice (Fig. 3). Such lines are called transects. Google Earth Pro was used for checking purposes (Fig. 4). Calculations were made for all seas in the Arctic region for each summer month from 2009 to 2019. The results are summarised in Table 2, where 0 means ice-free water.

June is characterized by maximum fast ice widths. The greatest sea ice melting occurs in July, which is quite noticeable in the seas of the Russian Arctic. In August, the melting rate slows down significantly.

The Greenland Sea is characterized by minimal reductions in the fast ice width. The maximum difference between June and August is 1/3 of the length, while in other areas the ice melts almost completely.

The coordinates of the ice edge position were taken for each of the seas using Google Earth. The results are recorded in Table 3.

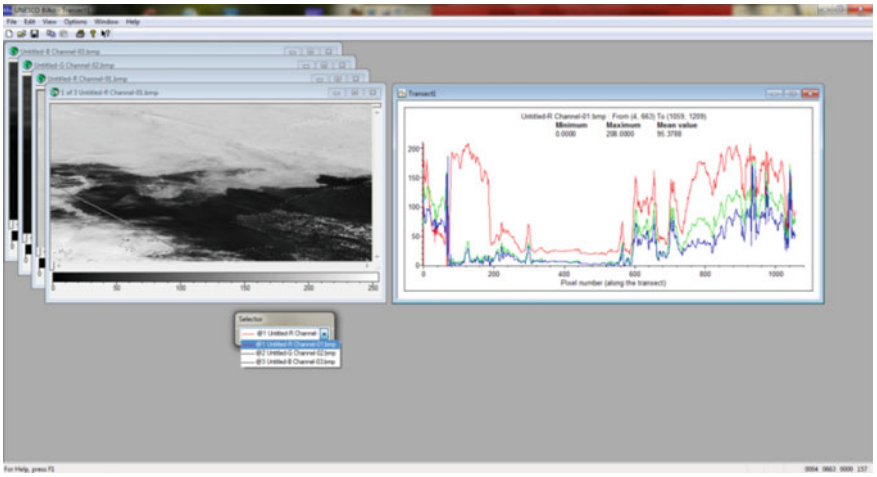

Fig. 3 The process of determining the fast ice width in the Chukchi Sea on a selected transect in the UNESCO Bilko software (July 4, 2009)

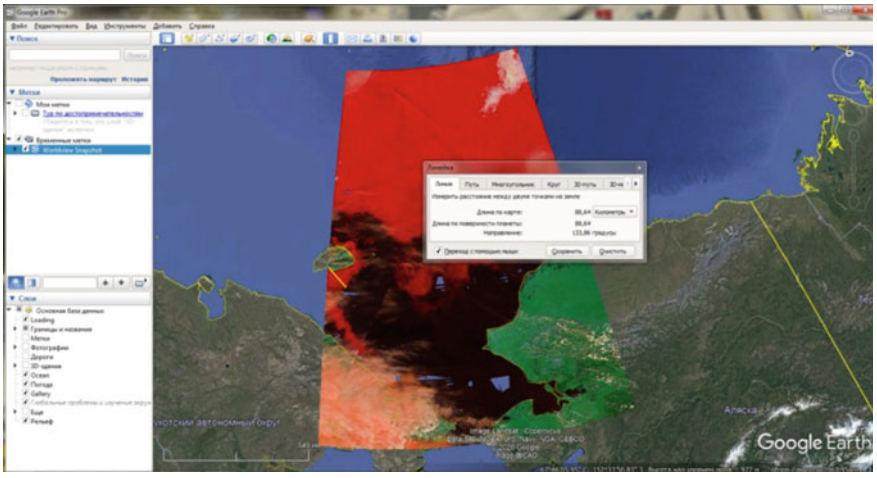

Fig. 4 The process of determining the length of the ice edge in the Chukchi Sea (in the highlighted section) using Google Earth (July 4, 2009)

According to the results obtained, the ice edge is in constant motion –summer melting shifts the southern ice edge closer and closer to the pole. At the same time, melting during the season occurs at different rates, which is determined by the geographical peculiarities of the area. Thus, the most pronounced change in the position of the ice edge during the summer months occurs in the Greenland, East

Table 2 Received results of fast ice width (in kilometers) for the Arctic seas during the summer period

Year	Month	Sea											
		East Siberian	Kara	Beaufort	Laptev	Chukchi	Baffin	Barents	White	Greenland	Norwegian	Bering	Labrador
2009	*VI*	160	247	390	404	211	496	195	0	395	0	47	136
	VII	140	189	129	292	88	156	18	0	383	0	0	11
	VIII	0	0	25	20	0	26	0	0	119	0	0	0
2010	*VI*	177	204	335	400	530	394	74	0	421	0	36	149
	VII	148	84	227	358	200	343	49	0	365	0	0	33
	VIII	73	0	174	5	15	283	0	0	287	0	0	0
2011	*VI*	150	210	357	388	393	499	50	0	391	0	41	87
	VII	115	75	321	282	174	381	47	0	372	0	0	25
	VIII	0	0	171	0	0	35	0	0	281	0	0	0
2012	*VI*	161	43	183	404	323	536	15	0	416	0	64	152
	VII	123	0	12	88	201	84	0	0	374	0	0	55
	VIII	120	0	0	0	130	0	0	0	288	0	0	0
2013	*VI*	223	245	477	282	423	572	158	0	386	0	39	191
	VII	166	166	395	270	119	313	0	0	163	0	0	73
	VIII	85	0	97	0	–	0	0	0	128	0	0	10
2014	*VI*	136	205	389	395	169	–	14	0	392	0	50	126
	VII	11	63	73	140	40	228	0	0	276	0	0	28
	VIII	5	0	0	0	36	0	0	0	259	0	0	0
2015	*VI*	103	158	203	332	243	446	265	0	259	0	5	226
	VII	16	82	187	47	154	365	214	0	196	0	0	193

(continued)

Table 2 (continued)

Year	Month	Sea											
		East Siberian	Kara	Beaufort	Laptev	Chukchi	Baffin	Barents	White	Greenland	Norwegian	Bering	Labrador
	VIII	0	0	149	0	0	–	0	0	133	0	0	90
2016	*VI*	135	38	359	350	335	533	17	0	271	0	37	114
	VII	83	0	321	90	198	246	0	0	178	0	0	104
	VIII	10	0	125	0	0	117	0	0	132	0	0	15
2017	*VI*	86	81	62	401	234	477	230	0	363	0	45	226
	VII	55	35	39	62	90	297	217	0	338	0	0	142
	VIII	0	0	0	20	0	112	0	0	258	0	0	24
2018	*VI*	99	201	345	390	297	676	20	0	261	0	0	216
	VII	67	49	335	–	86	457	0	0	201	0	0	105
	VIII	0	0	263	0	0	0	0	0	167	0	0	0
2019	*VI*	148	138	101	391	239	443	238	0	260	0	98	211
	VII	6	0	52	–	97	143	189	0	257	0	0	15
	VIII	0	0	14	0	0	0	122	0	249	0	0	0

Table 3 Edge position coordinates for the Arctic seas during the summer period

Year	Sea						
	Greenland	Barents	Kara	Laptev	East Siberian	Chukchi	Beaufort
June							
2009	71° 53′ N	73° 12′ N	75° 2′ N	74° 20′ N	69° 44′ N	70° 3′ N	70° 53′ N
2010	72° 29′ N	72° 16′ N	73° 10′ N	72° 17′ N	69° 44′ N	69° 23′ N	72° 18′ N
2011	72° 19′ N	73° 14′ N	74° 26′ N	73° 46′ N	70° 46′ N	71° 26′ N	71° 12′ N
2012	73° 6′ N	74° 33′ N	75° 40′ N	75° 4′ N	72° 1′ N	69° 37′ N	72° 15′ N
2013	74° 39′ N	76° 41′ N	76° 47′ N	74° 49′ N	71° 57′ N	68° 49′ N	70° 28′ N
2014	75° 52′ N	76° 2′ N	76° 11′ N	75° 22′ N	72° 15′ N	71° 51′ N	73° 4′ N
2015	75° 11′ N	81° 11′ N	78° 2′ N	76° 13′ N	73° 0′ N	70° 3′ N	73° 24′ N
2016	76° 24′ N	81° 47′ N	77° 7′ N	75° 1′ N	75° 6′ N	71° 4′ N	72° 58′ N
2017	74° 19′ N	79° 58′ N	79° 51′ N	77° 5′ N	76° 58′ N	71° 43′ N	73° 45′ N
2018	76° 8′ N	82° 8′ N	79° 20′ N	78° 8′ N	77° 16′ N	71° 36′ N	72° 49′ N
2019	77° 9′ N	82° 6′ N	78° 32′ N	79° 13′ N	77° 6′ N	72° 0′ N	73° 5′ N
July							
2009	73° 6′ N	74° 31′ N	75° 45′ N	76° 37′ N	72° 14′ N	71° 37′ N	71° 42′ N
2010	74° 0′ N	76° 33′ N	76° 2′ N	77° 43′ N	73° 24′ N	70° 58′ N	74° 23′ N
2011	74° 29′ N	75° 8′ N	76° 30′ N	77° 15′ N	72° 4′ N	72° 35′ N	71° 48′ N
2012	75° 18′ N	76° 12′ N	77° 1′ N	76° 14′ N	73° 6′ N	71° 36′ N	74° 26′ N
2013	74° 21′ N	77° 11′ N	77° 55′ N	78° 2′ N	75° 11′ N	69° 22′ N	71° 5′ N
2014	76° 43′ N	77° 42′ N	76° 45′ N	77° 13′ N	74° 23′ N	72° 18′ N	74° 33′ N
2015	77° 29′ N	78° 32′ N	78° 54′ N	77° 21′ N	75° 24′ N	71° 45′ N	74° 8′ N
2016	78° 32′ N	81° 52′ N	77° 49′ N	79° 5′ N	76° 3′ N	71° 46′ N	73° 17′ N
2017	80° 9′ N	80° 17′ N	80° 4′ N	78° 43′ N	78° 24′ N	72° 47′ N	73° 53′ N

(continued)

Table 3 (continued)

Year	Sea						
	Greenland	Barents	Kara	Laptev	East Siberian	Chukchi	Beaufort
2018	81° 33′ N	82° 22′ N	81° 7′ N	79° 11′ N	77° 5′ N	73° 35′ N	73° 9′ N
2019	82° 9′ N	82° 11′ N	80° 4′ N	80° 13′ N	78° 13′ N	72° 51′ N	74° 0′ N
August							
2009	74° 11′ N	75° 48′ N	76° 20′ N	77° 10′ N	74° 2′ N	72° 57′ N	72° 6′ N
2010	75° 19′ N	78° 43′ N	76° 58′ N	78° 6′ N	75° 49′ N	71° 43′ N	75° 7′ N
2011	76° 4′ N	77° 33′ N	78° 7′ N	79° 53′ N	74° 54′ N	72° 55′ N	73° 9′ N
2012	77° 13′ N	80° 42′ N	77° 21′ N	77° 51′ N	75° 29′ N	72° 50′ N	75° 5′ N
2013	75° 12′ N	79° 31′ N	77° 5′ N	79° 3′ N	77° 8′ N	70° 3′ N	72° 18′ N
2014	77° 11′ N	80° 1′ N	79° 8′ N	79° 10′ N	76° 45′ N	72° 36′ N	75° 21′ N
2015	78° 9′ N	81° 6′ N	78° 15′ N	80° 17′ N	77° 2′ N	74° 22′ N	74° 59′ N
2016	80° 19′ N	82° 4′ N	78° 37′ N	81° 33′ N	78° 51′ N	73° 5′ N	73° 41′ N
2017	82° 58′ N	81° 31′ N	77° 4′ N	80° 9′ N	79° 2′ N	74° 0′ N	75° 1′ N
2018	83° 57′ N	83° 9′ N	80° 22′ N	81° 12′ N	79° 34′ N	73° 19′ N	74° 1′ N
2019	84° 9′ N	83° 42′ N	82° 20′ N	81° 53′ N	80° 8′ N	74° 3′ N	74° 58′ N
Longitude	16° 55′ W	21° 13′ E	59° 31′ E	134° 23′ E	177° 32′ E	173° 15′ W	127° 26′ W

Siberian and Laptev Seas. The position of sea ice edge shifts on average approximately 458, 449 and 441 km between the sixth and eighth month of the year for the above-mentioned seas.

Regarding the temporal variability on a large scale, namely between 2009 and 2019, it is worth noting that the difference is strongest between August of the first year and the last year. The edge position lines presented in Fig. 5 are relatively similarly located along the entire border in June. At the same time, August is characterized by a stronger shift of the edge towards the north in the eastern Arctic.

We also classify winter seasons of the Russian Arctic seas by their severity. At first, the data, which represent the daily values of atmospheric temperature in the Arctic seas, were used for calculating the cumulative freezing-degree days (CFDD). At the second stage, the results were summarized in dendrograms using Ward's hierarchical clustering method.

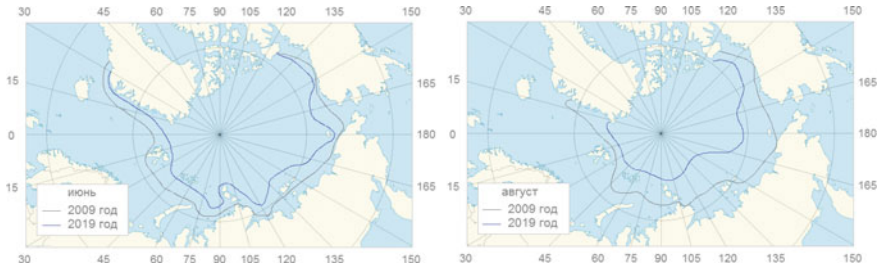

Fig. 5 Arctic residual ice edge position

The White Sea. In this research, we summarized negative air temperatures of winter seasons from Arkhangelsk in the period from 1885 to 2005. As a result, the following classification was obtained according to the severity of winter [10]: mild winter—up to 1052 CFDD, moderate winter—1053–1578 CFDD, severe winter—more than 1579 CFDD. The minimum value recorded in the winter of 1936/37 is 760 CFDD. The maximum value recorded in the winter of 1901/02 is 2288 CFDD. During the study period, moderate winters were observed in 57% of cases, while severe and mild winters—in 33% and 10%, respectively.

The Kara Sea. To classify the severity of winters in the Kara Sea, meteorological data from 1978 to 2017 from the port Dickson were used. As a result, the following classification of winters was obtained [11]: mild winter—up to 3300 CFDD, moderate winter—3301–4500 CFDD, severe winter—more than 4501 CFDD. It should be noted that in the period from 2004 to 2016, there was no severe winter, while a mild winter with a minimum value of 2058 CFDD was recorded in the winter of 2013/14. The maximum value recorded in the winter of 1978/79 was 5426 CFDD. During the study period, mild winters were observed in 46% of cases, severe winters—in 36% and mild winters—in 18%. It should be noted that mild winters have been recorded since 1993–94, while severe winters have not been recorded since 2004.

The Laptev Sea. To classify the severity of winters in the Laptev Sea, weather data from meteorological station Tiksi in the period from 1936 to 2018 were used. As a result, the following classification of winters was obtained: mild winter—up to 4900 CFDD, moderate winter—4901–5650 CFDD, severe winter—more than 5651 CFDD. The minimum value—4454 CFDD was recorded in the winter of 1942/43. The maximum value - 6210 CFDD was recorded in the winter of 1940/41. During the study period, mild winters were observed in 64% of cases, while severe and mild winters—in 20% and 16%, respectively. It should be noted that in the period from 2004 to 2017 there was no severe winter, and in the period from 2013 to 2016 there were only mild winters.

The East Siberian Sea. To classify the severity of winters in the East Siberian Sea, meteorological data from the weather achieve on Wrangel Island were used in the period from 1960 to 2017. As a result, the following classification of winters was obtained: mild winter—up to 3850 CFDD, moderate winter—3851–4500 CFDD,

severe winter—more than 4501 CFDD. The minimum value 2649 CFDD was recorded in the winter of 2017/18. The maximum value 4957 CFDD was recorded in the winter of 1975/76. During the study period, mild winters were observed in 57% of cases, while mild winters—in 33% and severe winters—in only 10% of cases. It should be noted that in the period from 1984 to 2017 no severe winters were recorded, and from 2001 to 2017 only mild winters were recorded.

Summing up, we can say that the decrease in the sea ice area and fast ice width is directly related to climate change in the Arctic region. The results are consistent with the presented classification, which shows an increase in mild winters in the Arctic seas during the period under investigation.

References

1. Kostyanoi A.G. Sputnikovyi monitoring klimaticheskih parametrov okeana. Chast' 1. [Satellite monitoring of the ocean climate parameters. Part 1.]. *Fundamental'naya i prikladnaya klimatologiya [Fundamental and Applied Climatology(Russia)]*, 2017, vol. 2, pp. 63–85. (In Russian; abstract in English).
2. Sputnikovye metody opredeleniia kharakteristik ledianogo pokrova morei. Satellite methods for determination of sea ice cover characteristics. Ed by V.G. Smirnov. St. Petersburg, AARI Edition, 2011, 239 p. (In Russian).
3. Repina I.A., Ivanov V.V. Primenenie metodov distancionnogo zondirovaniya v issledovanii dinamiki ledyanogo pokrova i sovremennoi klimaticheskoi izmenchivosti Arktiki. [Application of remote sensing methods in the study of ice cover dynamics and current climate variability in the Arctic]. *Sovremennye problemy distantsionnogo zondirovaniya Zemli iz kosmosa [Modern problems of remote sensing of the Earth from space]*, 2012, vol.9, pp. 89–103. (In Russian).
4. Bukatov A. E., Bukatov A. A., Babii M. V. Prostranstvenno-vremennaya izmenchivost' rasprostraneniya morskogo l'da v Arktike. [Spatial and temporal variability of sea ice distribution in the Arctic]. *Kriosfera Zemli [Earth's cryosphere]*, 2017, vol. 21, pp. 85–92. (In Russian).
5. Smirnov V. G., Bushuev A. V., Bychkova I. A., Zahvatkina N. YU., Loshchilov V. S. Sputnikovyi monitoring morskih l'dov. [Satellite monitoring of sea ice]. *Problemy Arktiki i Antarktiki [Problems of the Arctic and Antarctic]*. Issue 85. St. Petersburg: Gidrometeoizdat, 2010, pp. 62–75. (In Russian).
6. National Snow and Ice Data Center. Available at: https://nsidc.org/data/seaice_index/ (Accessed 02.06.2020).
7. EOSDIS Worldview. Available at: https://worldview.earthdata.nasa.gov (Accessed 10.06.2020).
8. EarthExplorer. USGS. Available at: https://earthexplorer.usgs.gov/ (Accessed 10.06.2020).
9. Teider M.S., Oskotskaia S.A., Frolova N.S., Podrezova N.A. The assessment of Arctic sea ice area changes. Springer proceedings in Earth and Environmental Sciences. 2022, pp. 231–241.
10. Sergeev D.I., Podrezova N.A. Calculation of ice growing in the White Sea in conditions of mild, moderate and severe winter. Meteorologicheskii Vestnik [The Meteorological Bulletin], 2017, vol. 9, no. 2, pp.187-190 (In Russian).
11. Petruchenko A.I., Kruglova E.E., Mechova O.S., Podrezova N.A. Assessment of sea ice changes in the Kara Sea depending on the severity of winter. Trudy IX Mezhdunarodnoi nauchno-prakticheskoi konferentsii «Morskie issledovaniia i obrazovanie» [Proc. of the IX International Scientific and Practical Conference «Marine Research and Education»]. Tver, 2020, pp. 273–274. (In Russian).